ISSN (Online) 2456-1290

International Journal of Engineering Research in Mechanical and Civil Engineering (IJERMCE)

Vol 10, Issue 10, October 2023

Investigation of Robotic Deburring for Enhanced Surface Quality using Force/Torque Sensor

[1] Ankul Lohiya, [2] Gagan Preet Kaur, [3] Gaurav Srivastava, [4] Dr. Manoj Kumar Yadav

[1][2][4] Department of Mechanical Engineering, Ajay Kumar Garg Engineering College, Ghaziabad, Uttar Pradesh, India
[3] Department of Electrical & Electronics Engineering, Ajay Kumar Garg Engineering College, Ghaziabad, Uttar Pradesh, India
Email: [1] ankul214004-m@akgec.ac.in, [2] kaurgaganpreet@akgec.ac.in, [3] srivastavagaurv@akgec.ac.in, [4] yadavmanoj@akgec.ac.in

Abstract*— Robotics becomes very important in the industrial sector because it increases productivity and accuracy. The robotic deburring is one of major application used in manufacturing industries to remove burrs from casting of machined parts with accuracy and precisely. The deburring forces acting during the process, applied by the robot's end-effector are monitored and controlled in this work by the use of force/ torque sensors. The sensors gives real-time feedback that can be used to optimize the input parameters to prevent under- or over-deburring. The advantages of this strategy includes better surface quality, decreased tool wear, and increased process reliability. The results highlight how the force and torque sensing may advance robotic deburring. In the proposed study exceptionally high force values (F_x, F_y, F_z) and torque values (T_x, T_y, T_z) was observed with the rotational speed of 42000 rpm, feed rate 50 mm/s and with double cut tool geometry. The average roughness falls in the range of 2.2 µm to 3.7 µm which indicates that tool geometry, spindle speed and feed rate play critical roles to get the desired output.

***Index Terms*— Deburring, Force & Torque sensor, KUKA KR-6 Robot, Robotic deburring, Surface Roughness**

I. INTRODUCTION

The use of bots in the present manufacturing process, their current status, the barriers to their acceptance, and related information. It emphasises the significance of modelling and identification for robot-assisted machining process optimisation, planning, and control. Verl et al. discussed in the paper focuses on a variety of machining operations where robots must efficiently manage significant process pressures, including deburring, milling, incremental shaping, polishing, and thin-wall machining **[1].** Schimmels et al. improved positioning capability and increasing the efficient rigidity (bracing) of a robot manipulator by utilising multifaceted compliance and limitation **[2].** Ke. X et al. investigated the finishing, such as versatility in work ranges as well as a low cost contrasted to conventional techniques, are highlighted by recent advances in robot-assisted buffing technology in order which are widely utilised in accuracy sectors like biological medicine, photonics, and optics **[3].** Kuss A. et al. defined the use of work-piece form deviations to identify shape variations in robotic deburring procedures. For planning the trajectory and work-piece localisation, it matches point clouds and determines the most comparable geometry model using dimensional tolerance criteria and an Iteration Closest Point (ICP) method **[4].** Schmidt et al. developed a zero Defect clever deburring robotic cells with a unique architecture. Because of the unpredictability of burrs, it is essential to automate the deburring process whenever high quality is required. That was successfully designed and proven to determine the best order of operations and operating conditions to achieve the target quality **[5].** Pires et al. developed an indirect control of force technique for applications involving industrial robotic deburring, especially for premium knives. Because of concentration issues, the Robotic systems can achieve the necessary level of accuracy in the deburring operation thanks to the recommended technique **[6].** Princely et al. presented a way for programming a deburring robot for batch production using a vision-guided robotics system (VGRS). That provides a small and reasonably priced finishing robot system and considerably cuts down on programming time, is confirmed by experimentation with the robot system **[7].** Shukla. et al. examined the best welding techniques to use while employing wire arc additive manufacturing (WAAM) technology to create thin walls with a smooth surface of ER70S-6 steel weld beads. The study combines the use of a welding robot, a CMT power source, and WAAM technology **[8].** Grandi. et al. proposed a revolutionary design for intelligent robotic cells for zero-defect deburring. The metrological sensors to detect burrs and determine the quality of the work piece **[5].** Wang et al. designed a completely pre-stressed, six-axis, double-layered force/torque sensor was created and tested. In this a calibration method is created, and a sensor prototype is produced **[9].** Caesarendra et al. made a sensor data analysis tool to measure and link the deburring stage to the quality of the surface finish in the production of aerospace components. An adaptive neural-fuzzy inference system (ANFIS) is used to analyse the retrieved characteristics and forecast the exterior finishing level in terms of head hole chamfer length and deburring process stage classification **[10].** Winkler et al. emphasised the rising role of force/torque control over

ISSN (Online) 2456-1290

International Journal of Engineering Research in Mechanical and Civil Engineering (IJERMCE)

Vol 10, Issue 10, October 2023

manufacturing activities. A single robot mounts a nut on a threaded bolt utilising hybrid position/force control in the first experiment, while two collaborating robots build a screw fitting using force/torque control in the second **[11].** MacMillan W. R et al. suggested the Planar Image-Space Trajectory (PIST) design method for force control and contour following to provide force control, the PIST algorithm creates machining paths offsets to a flat piece of metal with a force being applied direction. A real-life instance of deburring parts from sheet metal using the algorithm and CAD/CAM software is used to validate it **[12].** Lloyd et al. utilised a Denso VS-6556G manipulator for robotic deburring operations, provided the modelling, testing, and evaluation of the pseudo-symbolic dynamic modelling (PSDM) technique. PSDM evaluate dynamic models in real-time and delivers them in a retrograde for 98–100% of the effects of the motor, gravity, and friction, and accounting for 81–99% of the reported torque effects through high-speed acceleration fitting **[13].** Verl et al. emphasised the benefits of robotic machining centres, including their cost-effectiveness, capacity to reconfigure themselves, and vast operation reach **[1].** J.E. et al. created a collaboration between humans and robots for jobs like deburring, grinding, and polishing surfaces. The method is based on adaptable unconventional sliding mode control & the efficacy and adaptability of the suggested strategy are demonstrated by experimental results utilising the redundant 7R Sawyer cobot **[14].** Garcia et al. outlined an innovative strategy for performing surface treatment procedures that combines human-robot cooperation for the best results **[15].** Guillo et al. investigated on Friction Stir Welding (FSW), and looked at an industrial serial robot to cut costs and improve process flexibility. According it, a robot equipped with an actual time compensation algorithm may produce FSW with an equivalent level of quality as a CNC gantry system **[16].** Hu et al. offered the dual-edge chamfering technique, a unique approach to robotic gear chamfering that allows for simultaneous chamfering of neighbouring gear tooth edges and corrects common registration issues in the robot workspace **[17].** Hjorth et al. developed the idea of resource recycling and sustainable human-robot collaboration during disassembly. It also reviewed technical difficulties and the systems that now support HRCD **[18].** Mukherjee et al. highlighted the introduction of human-robot cooperation (HRC) in industry to meet the growing need for flexible production. It presents broad descriptions of several forms of machine learning and discusses the channels of HRC fuelled by machine learning **[19].** Gotlih J et al. focused on improving robotic deburring processes for industrial automation. That integrates a rotary table to extend the robot's reach and employs a genetic algorithm to optimize workpiece. An artificial neural network (ANN) models robot stiffness **[20].** Jia et al. shifted from traditional manual grinding to robotic grinding for accurate material removal that was a challenge for workpieces with complex profiles. In it a prediction model of the blade material removal depth (MRD) was established, based on the Adaptive Neuro-Fuzzy Inference System (ANFIS) using the Taguchi method and Analysis of Variance (ANOVA). The mean absolute percent error (MAPE) of the established ANFIS model, after training and testing, was 3.976%, demonstrating superior performance to the reported findings, which range from 4.373% to 7.960%. ANFIS exhibited superior outcomes, when compared to other prediction models, such as random forest (RF), artificial neural network (ANN), and support vector regression (SVR) **[21].** Guo et al. explored the advancements in the field of industrial robotics, particularly focusing on the benefits of industrial robots for automation solutions. It outlines a methodology for planning tool paths and controlling process parameters in robotic deburring, employing fuzzy control **[22].** Very limited work is available on the optimization of the process parameter using artificial neural network for the robotic deburring operation with the variation of tool geometry and other process parameters. In the proposed work, the study was performed with the tool geometry variation along with spindle speed and feed rate. The work compiled the variation in output with the change of set of input parameters.

II. METHODOLOGY

The robotic deburring setup incorporating a force and torque sensor (F/T sensor) is a critical component for achieving precise and adaptable deburring operations. This setup requires the installation of the F/T sensor at the end effector of the robot's flange, specifically a KUKA KR-6 robot, to ensure the accuracy and effectiveness of the deburring process.

The Force/Torque sensor is strategically positioned on the robot's end-effector, enabling it to continuously monitor the forces and torques generated as the deburring tool interacts with the workpiece during the deburring process. This real-time monitoring allows for the immediate detection of any excessive forces or torques, which can then be precisely described and analysed using the F/T sensor.

The integration of the Force/Torque sensor is seamlessly achieved on the KUKA KR-6 manipulator, as depicted in Figure-2, and is controlled through the C4 compact-size controller. Real-time data and human interaction are facilitated by the F/T Data Viewer software. This software acts as a communication bridge between the Force/Torque sensor and the robot's motion control system, providing exact values of the applied force and torque in all respective directions.

Following the integration of the F/T sensor at the end effector of the robot, the "FDB-340" Deburring spindle, as detailed in Table-01, is securely attached using an adaptor plate. This pneumatically operated spindle operates at 6-bar of pressure and is specifically designed for X and Y-direction compensation during the deburring process, with a maximum

ISSN (Online) 2456-1290

International Journal of Engineering Research in Mechanical and Civil Engineering (IJERMCE)

Vol 10, Issue 10, October 2023

compensation range of ±7.5 mm, as outlined in Table-01. The FDB-340 spindle features two pneumatic ports, one with a 10mm connection to control spindle speed ranging from 42000 to 65000 rpm and the other with a 4mm connection for locking the compensation mechanism.

The integration of the Force/Torque sensor into the robotic deburring setup, coupled with the FDB-340 Deburring spindle, transforms the KUKA KR-6 robot into a highly adaptable and precise deburring solution. This setup is equipped to handle various workpiece shapes while ensuring optimal deburring effectiveness and quality. The real-time monitoring and control provided by the Force/Torque sensor, facilitated by the F/T Data Viewer software, contribute to the overall efficiency and reliability of the deburring process.

Table 1: Specifications of FDB-340, Deburring spindle.

Compensation XY	7.6 mm
Max. compensation X	± 7.5 mm
Max. compensation Y	± 7.5 mm
Schunk Gamma Series	FT2460

In deburring operation, two tool geometries for the burr removal process was used. These geometries are Double Cut and Alt Diamond Cut as shown in figure -1.

Figure 1(a): Tool Geometry of Double Cut, 1/4" Burr Dia, 3/4" Burr Length, 1/4" Shank.

Figure 1(b): Tool Geometry of Alt Diamond Cut, 1/4" Burr Dia., 3/4" Burr Length, 1/4" Shank.

The preference between the Double Cut tool and the Alt Diamond Cut tool shown in figure 1(a) and (b) respectively, involves a consideration of their respective cutting edge designs, inclination angles, and sharpening depths, which directly impact their deburring performance and the resulting surface roughness. The Double Cut tool, features a cutting edge with a smaller slope and a specific inclination angle. Additionally, it has a sharpening depth of 0.8mm. This design configuration enables it to remove burrs smoothly and efficiently, contributing to a better surface roughness outcome. The smaller slope and inclination angle allow for a more controlled and precise deburring process, which is particularly advantageous when fine-tuning surface finishes is a critical requirement. On the other hand the Alt Diamond Cut tool, boasts a larger slope cutting edge and a sharpening depth of 1.0mm. This design characteristic equips it with the ability to remove burrs more rapidly compared to the Double Cut tool. The larger slope allows for a more aggressive cutting action, making it adept at tackling burrs quickly. This rapid burr removal capability can be especially beneficial in scenarios where speed and efficiency are prioritized over achieving an extremely fine surface finish. The Double Cut tool excels in situations where precision and a superior surface finish are paramount, offering controlled and smooth burr removal. Conversely, the Alt Diamond Cut tool is the preferred choice when expediency is crucial, as it can swiftly eliminate burrs with its larger slope cutting edge and greater sharpening depth. The selection of the most suitable tool ultimately hinges on striking the right balance between deburring speed and surface finish quality to meet the desired outcome.

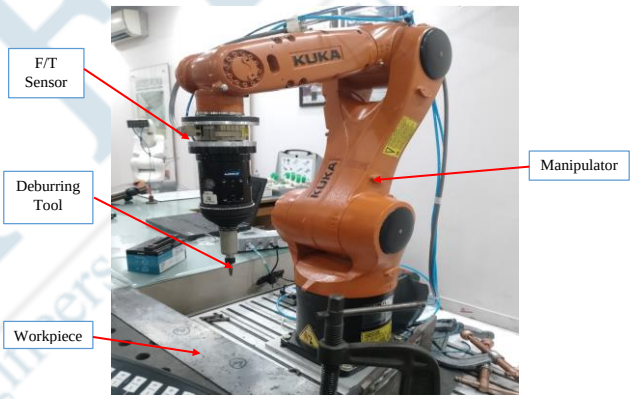

Figure 2(a): Robotic (KUKA KR-6) Deburring set-up with Force/Torque sensor

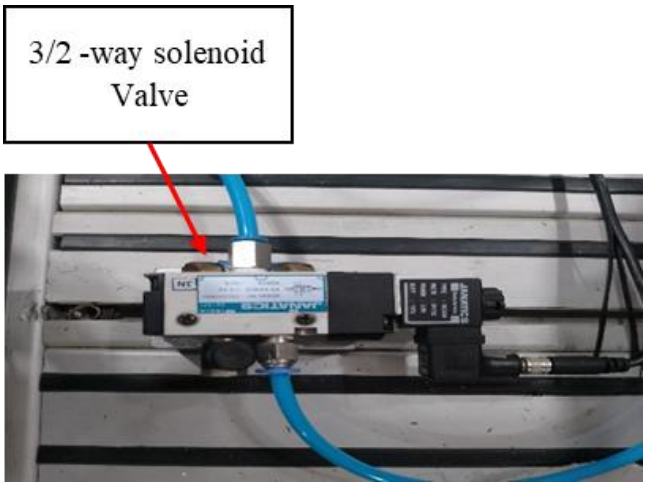

Figure 2(b): Solenoid valve.

ISSN (Online) 2456-1290

International Journal of Engineering Research in Mechanical and Civil Engineering (IJERMCE)

Vol 10, Issue 10, October 2023

Figure 2(c): Force/ Torque Net box.

The KUKA KR-6 robot serves as the foundation for automating the deburring procedures, and the inclusion of the Force/Torque sensor adds a crucial layer of input and control to this setup shown in figure-2. The KUKA KR-6 articulated manipulator to execute the deburring operation after mounting the F/T sensor and FDB deburring spindle at the end effector as shown in figure 2. A 3/2 way solenoid valve was used to operate the deburring spindle and Net Box was used to get the force and torque value in F/T data viewer software as depicted in figure 2(b) and (c) respectively.

The force/torque sensor is equipped with a comprehensive six-axis observation capability, enabling it to monitor forces and torques in three-dimensional space along the X, Y, and Z axes. It can detect forces acting in the horizontal X, Y and vertical Zs directions, as well as torques or rotational forces around these same axes. The sensor's ability to measure these six components of force and torque provides a holistic view of how external forces and moments interact with the object or system it is attached.

To achieve this precise observation, the inner hub of the force/torque sensor incorporates three pins, and each of these pins is equipped with four strain gauges. Strain gauges are specialized sensors that change their electrical resistance when subjected to mechanical deformation, such as the strain resulting from applied forces and torques. These strain gauges are strategically placed on each pin to detect variations in the strain caused by forces and torques in the X, Y, and Z directions. Specifically, there are four strain gauges on each pin, and they are arranged to monitor forces in the X (Fx), Y (Fy), and Z (Fz) directions, as well as torques around these axes (Tx, Ty, and Tz).

The strain gauges' ability to precisely measure these variations in resistance which allows the sensor to convert these electrical changes into accurate force and torque readings along each axis. As a result, the sensor can provide detailed insights into how external forces and moments affects the object or system it is attached to, making it an important tool in various applications, such as robotics, manufacturing, and materials testing, where understanding and controlling forces and torques are essential for optimal performance and safety. As shown in figure-3.

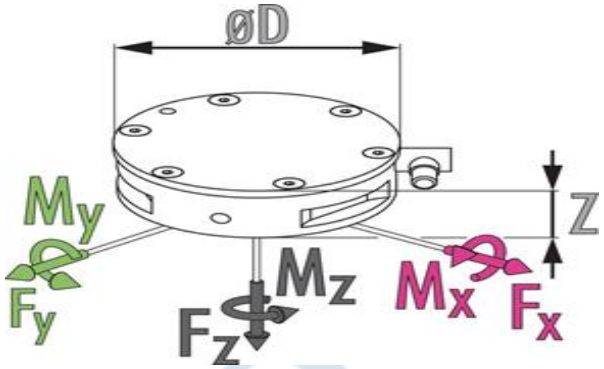

Figure 3: Force/Torque distribution direction in Schunk's F/T sensor [12].

The comprehensive setup for robotic deburring is characterized by a meticulous process that commences with the precise registration of the workpiece within the robotic workspace. Subsequently, the trajectory meticulously planned for the deburring tool assumes a pivotal role in determining the input parameters for the experiments. These parameters encompass crucial factors such as robotic arm speed, and tool orientation, all carefully tailored to achieve the desired deburring outcome. During the execution phase, the Force/Torque sensor continually monitors the interaction between the tool and the workpiece, providing real-time feedback on forces and torques. Collected data informs the evaluation and analysis of the deburring process, allowing for iterative adjustments as needed. Commonly, the efficacy of this setup is contingent upon the precision of workpiece registration and the strategic planning of the tool path, which directly influence the input parameters, and, consequently, the accuracy and repeatability of the deburring operation.

The experiments were performed on the basis of Taguchi L8 OA. The input parameters spindle speed, Feed Rate and Tool types were selected as shown in table-2. Total eight experiments were performed on the basis of the combination of parameters shown in table-2.

Table 2: Input parameters of Robotic deburring Process.

Exp. No.	Input Parameters		
	Spindle Speed (RPM)	Feed Rate (mm/sec)	Tool
1	65000	50	Double Cut
2	65000	38.8	Double Cut
3	65000	38.8	Alt Diamond Cut
4	65000	50	Alt Diamond Cut
5	42000	50	Alt Diamond Cut
6	42000	38.8	Alt Diamond Cut
7	42000	50	Double Cut
8	42000	38.8	Double Cut

The input parameters constitute the essential variables governing the robotic deburring process. These parameters encompass spindle speed, feed rate, and tool geometry, each playing a distinct role in shaping the efficiency and outcomes

ISSN (Online) 2456-1290

International Journal of Engineering Research in Mechanical and Civil Engineering (IJERMCE)

Vol 10, Issue 10, October 2023

of the operation. The spindle speed is meticulously controlled at two pneumatic pressure levels, offering the versatility to tailor the rotational velocity of the deburring tool for specific needs. Likewise, the choice between two feed rates, operating at 50% and 75% of the robot's speed, enables precise control over the robot's movement speed, influencing the pace and efficiency of material removal. Additionally, the selection between two deburring tool geometries, the Double Cut and Alt Diamond Cut, caters to varying deburring requirements, providing options for precision finishing or rapid burr removal. These input parameters collectively empower the customization and optimization of the deburring process, ensuring it aligns precisely with the desired surface finish and quality criteria for the work-piece.

After the deburring process, the roughness profile and surface roughness of the workpiece was measured through the roughness testing machine. The roughness of the deburred surface was quantified using a Zeiss measurement system, shown in figure 4. Average roughness (R_a) was calculated by adding the roughness measurements from the eight trials and the parent component measurement, effectively merging information from several sources.

Figure 4: Roughness testing machine.

This method gives a thorough way to assess the material's average surface roughness by including data from many tests and the parent material's baseline measurement, giving the surface quality of the material a more comprehensive view.

Mathematically, the average roughness (R_a) is defined as equation (1):

$$Ra = \frac{(\sum Ri)}{(n+1)} \quad \ldots\ldots\ldots\ldots\ldots \quad (1)$$

Where,

Ra: Average roughness; ΣRi: Sum of roughness values from all trials and the parent material and; n: Total number of data points.

To investigate the results with respect to the output force, torque and average roughness used the Taguchi technique.

III. RESULT AND DISCUSSION

Throughout the series of experiments, a force/torque sensor manufactured by Schunk was used to meticulously measure the forces and torques encountered by the deburring tool during the operation. Figures 5 to 12 vividly illustrate the intricate profiles of force and torque in three dimensions: X, Y, and Z for the experiment 1 to 8 respectively. For instance, Experiment 01 is exemplified in Figure 5, where we observed a force of 15.24 N acting in the X-direction, concurrently causing the torque in the Y-direction to fluctuate with a peak variation of 3.2 Newton-meters.

The underlying significance of monitoring and controlling the applied force during the deburring process cannot be overstated. It stands as the linchpin for the successful removal of burrs while safeguarding the integrity of the workpiece. The crux lies in maintaining an optimal force level, a delicate balance that ensures the deburring operation proceeds efficiently, culminating in a polished surface finish. This optimization prevents undue stress and strain on the workpiece, a paramount concern in precision deburring.

Turning our attention to Experiment 02, it was observed that the maximum force recorded in the X-direction was 13.5 N, which correspondingly led to the highest torque observed in the Y-direction, mirroring the peak torque variation of 3.2 Newton-meters. This trend in force and torque dynamics was documented in Figure 6. Experiment 03 introduced intriguing nuances. Here, we observed the maximum force applied in the X-direction to be 25.7 N, while concurrently encountering a reference negative force of -28.5 N in the Y-direction. These intricate variations in force across both the X and Y directions gave rise to matching maximum torque values, clocking in at 6.2 Newton-meters for the X-direction and 6.8 Newton-meters for the Y-direction, as artfully depicted in Figure 7.

ISSN (Online) 2456-1290

International Journal of Engineering Research in Mechanical and Civil Engineering (IJERMCE)

Vol 10, Issue 10, October 2023

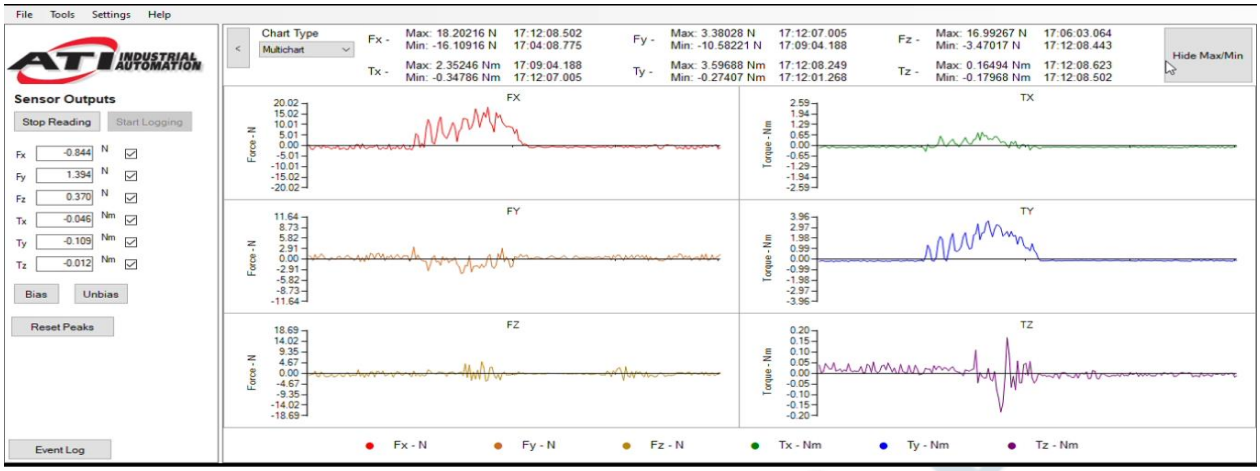

Figure 5: Force & Torque variation of experiment-1.

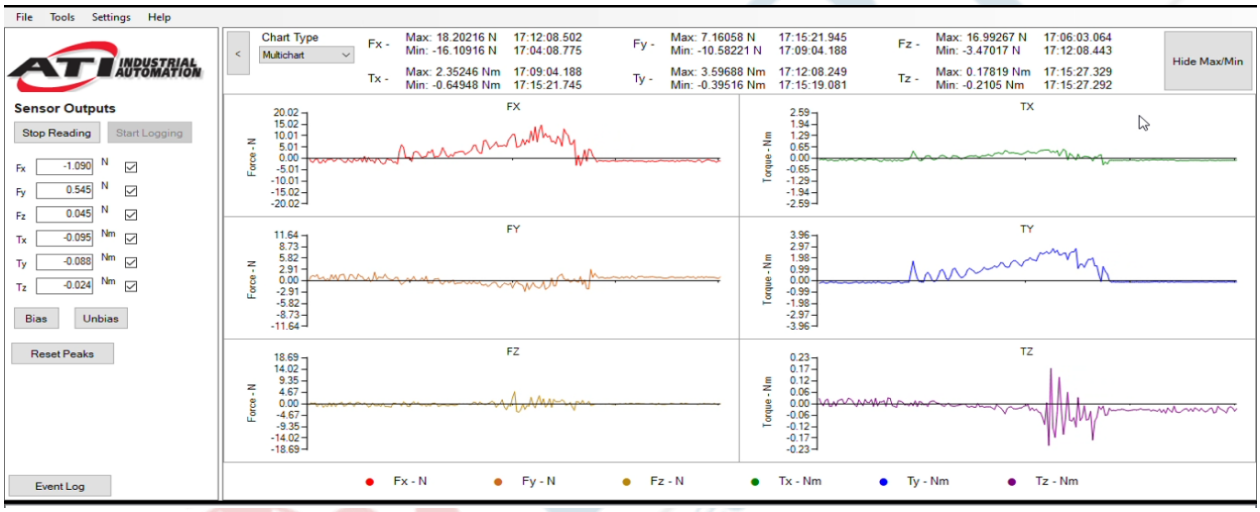

Figure 6: Force & Torque variation of experiment-2.

The meticulous observation and analysis of force and torque dynamics during these experiments underscore their pivotal role in achieving effective burr removal. Careful control of applied force not only ensures the desired surface finish but also acts as a guardian of the workpiece's structural integrity. The real-world application of these force and torque profiles in the context of deburring is indispensable for optimizing precision and quality in the machining process.

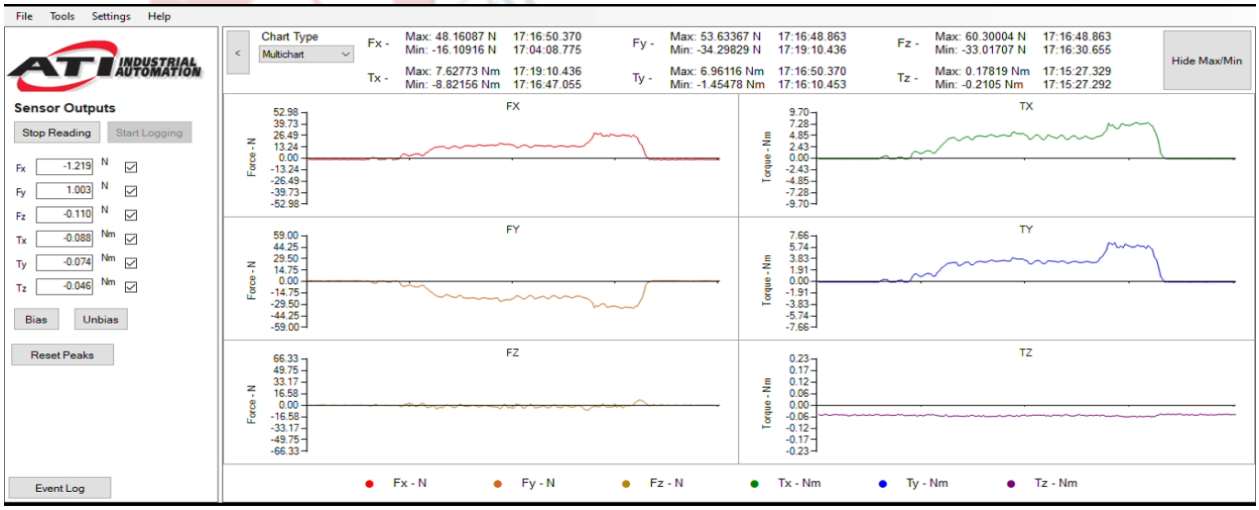

Figure 7: Force & Torque variation of experiment-3.

ISSN (Online) 2456-1290

International Journal of Engineering Research in Mechanical and Civil Engineering (IJERMCE)

Vol 10, Issue 10, October 2023

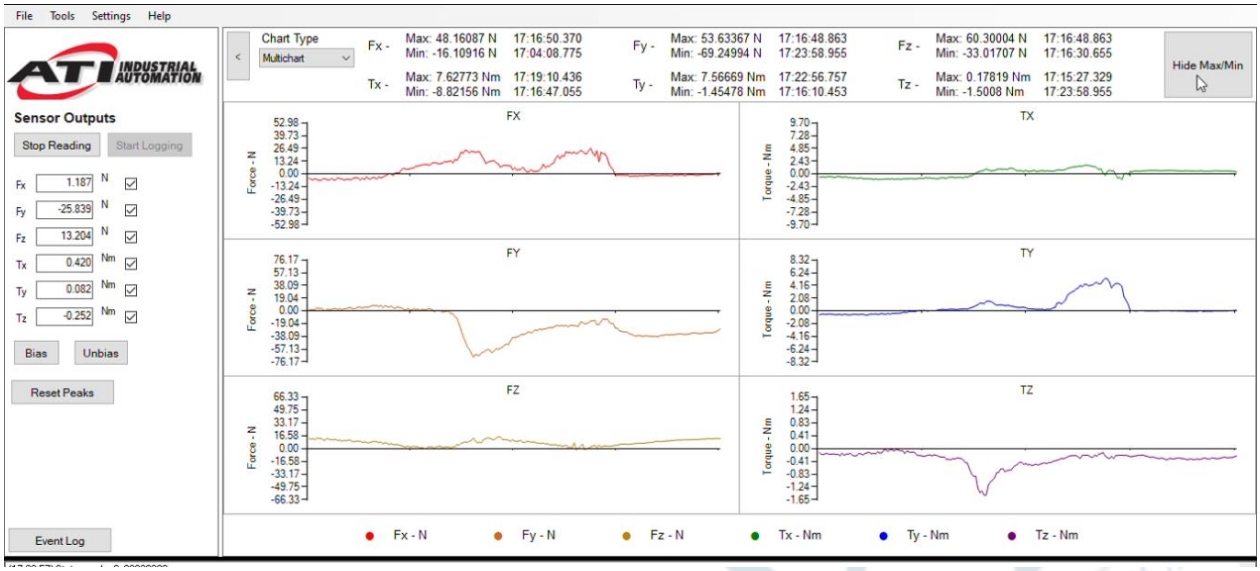

Figure 8: Force & Torque variation of experiment-4.

n Experiment 04, a detailed examination of force and torque dynamics during the deburring process revealed intriguing patterns. Positive force values were notably observed in the X and Z directions, indicating significant interactions between the deburring tool and the workpiece surface. However, the Y-direction stood out with a distinctive negative force of -56.7 N. This Y-direction force was a pivotal factor that instigated shifts in the torque values. Specifically, the torque value began at -1.65 Newton-meters but swiftly transitioned to a peak torque of 5.2 Newton-meters, as depicted in Figure-8.These observations underscore the intricate and multidimensional nature of forces and torques during deburring.

Experiment 05 introduced further complexities, with a focus on force variations primarily in the X-direction, where a force of 23.6 N was noted. This force variation resulted in compelling torque fluctuations within the XY-direction, spanning from 3.5 Newton-meters to 5.2 Newton-meters. Notably, the predominantly positive force in the X-direction corresponded with positive torque values in the Y-direction, as illustrated in Figure-9. This correlation between force and torque orientation highlights the interdependence of these parameters during the deburring process.

Experiment 06 continued to unveil insights into this intricate relationship. Here, the maximum force recorded in the X-direction, reaching 30.6 N, corresponded to the highest torque values in the Y-direction, peaking at 6.2 Newton-meters. These consistent trends persisted into Experiment 07, where force values progressively increased from 130 N to 197 N in the X-direction. This upward force trend was mirrored by concurrent rises in torque values, observed in both the X and Y directions, and reaching approximately 8.2 Newton-meters. These findings, encapsulated in Figure-11, underscore the critical role of precise and balanced force application in achieving high-quality deburring outcomes. Experiment 1 (higher feed rate) exhibits higher force values (Fx, Fy, Fz) compared to Experiment 2 (lower feed rate), indicating that an increase in feed rate generally leads to higher cutting forces. Similarly, Experiment 4 (higher feed rate) has higher force values than Experiment 3 (lower feed rate). Experiment 7 stands out with exceptionally high force values (Fx, Fy, Fz) and torque values (Tx, Ty, Tz). This is due to its extremely high feed rate and roughness Ra values in combination with a "Double Cut" tool geometry.

Comparing Experiments 1 and 2 (both using the "Double Cut" tool geometry), it was observed that they have similar spindle speeds and feed rates but slight variations in force and torque values. This suggests that factors like tool wear or material properties may contribute to the differences. Experiments 3, 4, 5, 6, 7, and 8 all use "Alt Diamond Cut" tool geometry, but their input and output values vary significantly. This indicates that tool geometry alone is not the sole determinant of force and torque; other factors such as roughness Spindle speed and feed rate play critical roles.

Lastly, in the context of an average roughness value of 3.672 micro meters (Figure-10), Experiment 07 exhibited force variations ranging from -25.6 N to 23.5 N, mirroring similar variations in torque values, which spanned from -1.2 Newton-meters to 4.7 Newton-meters (Figure-11). This comprehensive exploration of force and torque interactions emphasizes their significance in the deburring process's success, not only for achieving desired surface finish but also in safeguarding workpiece integrity. Ultimately, the optimization of force/torque parameters and the analysis of average surface roughness profiles serve as invaluable tools for gaining deeper insights into the observed data, further refining and enhancing the precision of the deburring process, as illustrated in Figure-12.

ISSN (Online) 2456-1290

International Journal of Engineering Research in Mechanical and Civil Engineering (IJERMCE)

Vol 10, Issue 10, October 2023

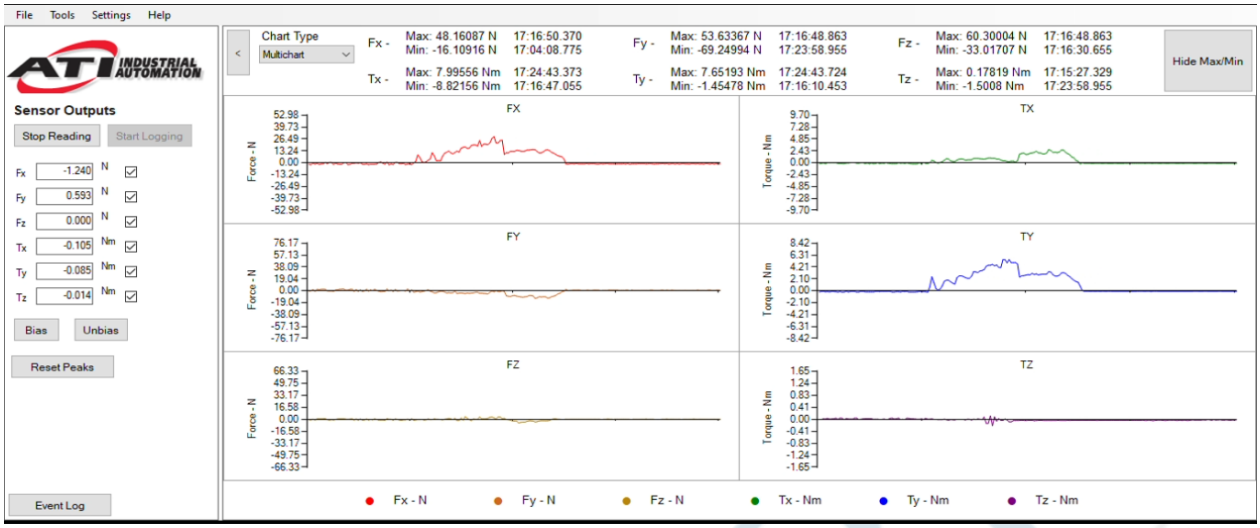

Figure 9: Force & Torque variation of experiment-5.

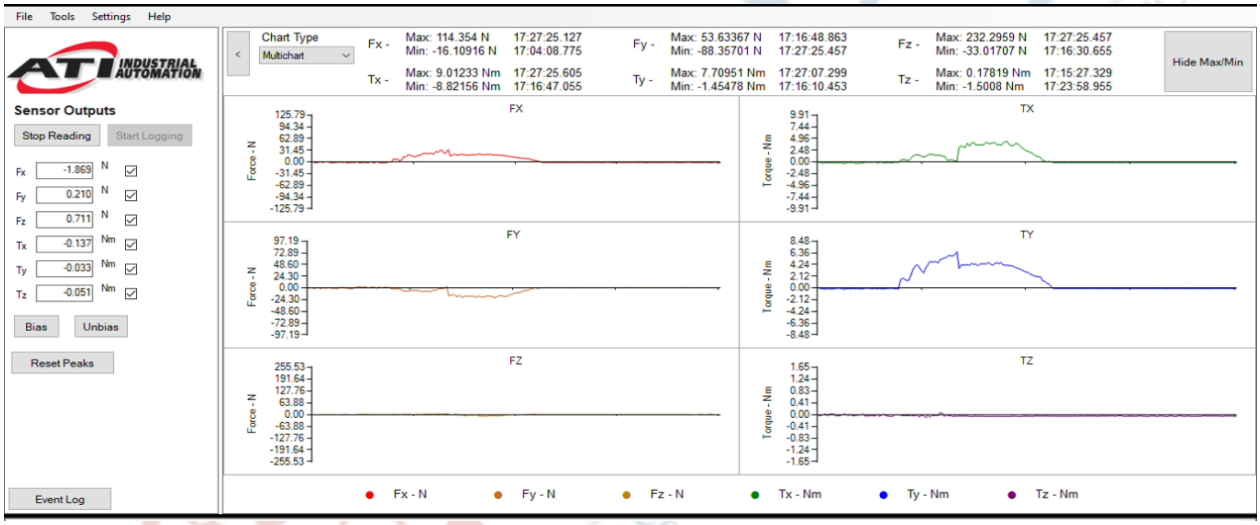

Figure 10: Force & Torque variation of experiment-6.

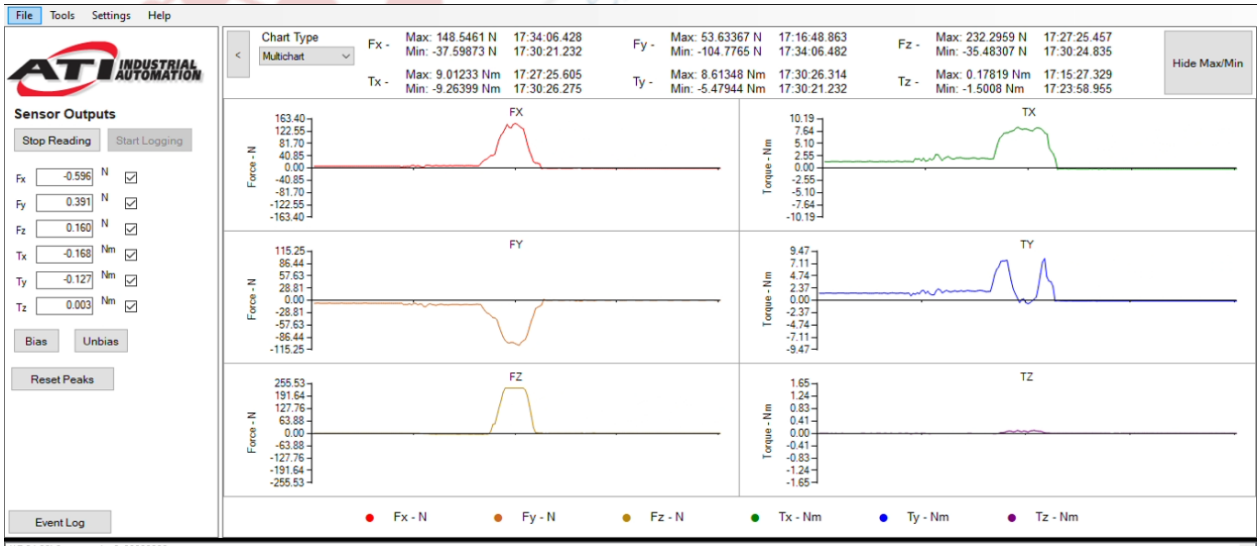

Figure 11: Force & Torque variation of experiment-7.

ISSN (Online) 2456-1290

International Journal of Engineering Research in Mechanical and Civil Engineering (IJERMCE)

Vol 10, Issue 10, October 2023

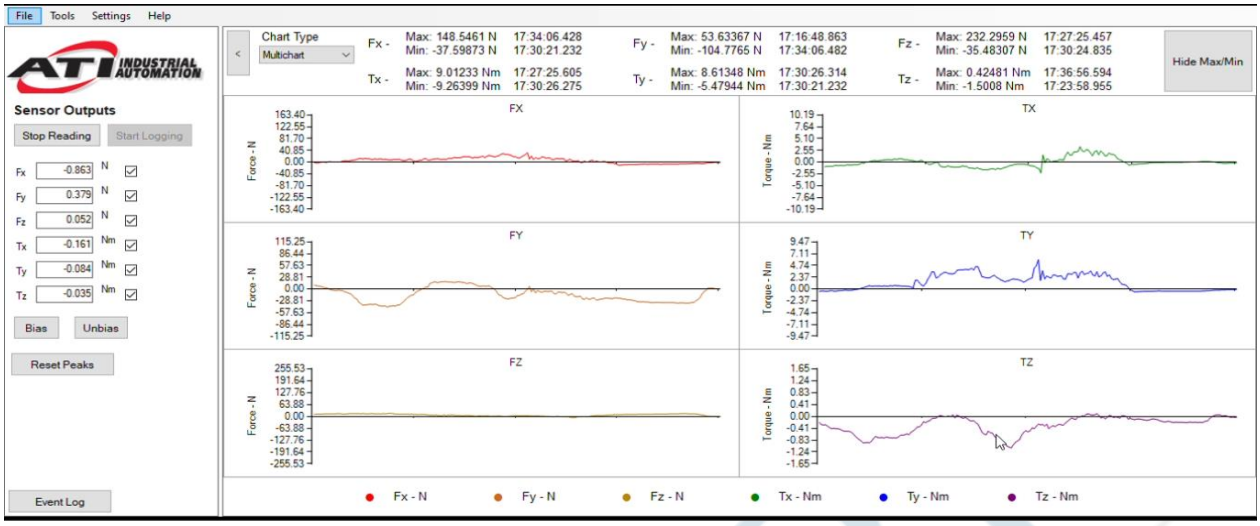

Figure 12: Force & Torque variation of experiment-8.

The results obtained from the series of deburring experiments consistently exhibited diverse values of force and torque, indicating the dynamic nature of the deburring process across all directions. These variations in force and torque were instrumental in shaping the surface roughness profile of the workpiece. Over the course of eight trials, a meticulous analysis of the data allowed for the calculation of the average roughness. This parameter provided critical insights into the quality of the deburring process. Notably, the average roughness values ranged from 2.2 µm to 3.7 µm, showcasing the versatility of this robotic deburring setup in achieving different levels of surface finish. The workpiece's roughness profile, as illustrated in Figure 13, specifically for Experiment 06, vividly showcases the microstructure profile resulting from the deburring operation. This visual representation of the workpiece's surface characteristics serves as a tangible testament to the precision and effectiveness of the deburring process, with the associated microstructure profile offering further insights into the fine details of the workpiece's surface profile. Experiment 4 has the highest roughness Ra (3.768 µm) among all experiments and exhibits significantly higher force and torque values. This demonstrates that a rougher workpiece surface requires more force and torque to achieve the desired finish.

These variations in force and torque values provide a comprehensive view of the intricate dynamics at play, highlighting the fine balance required for precise deburring. The calculated average roughness values across the eight trials reveal the adaptability of the deburring setup in achieving a range of surface finishes. The spindle speed parameters, set at 42,000 and 65,000 RPM, coupled with two distinct feed rates of 38.8 mm/sec and 50 mm/sec, in combination with the utilization of two different tool shapes, yielded a fascinating array of results, all contributing to the average roughness values ranging from 2.2 µm to 3.7 µm. This wide range of roughness values underscores the versatility of the robotic deburring setup in achieving various surface finishes, catering to specific quality requirements.

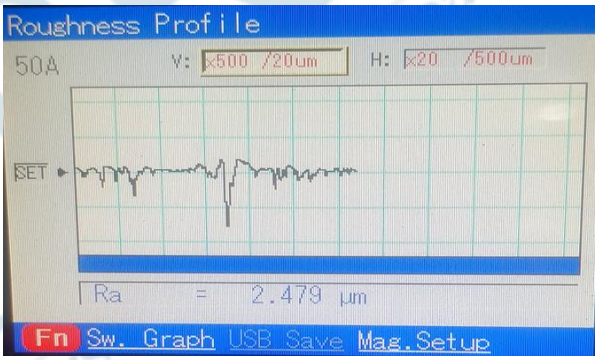

Figure 13: Roughness profile.

Involving into the specifics of the experiments, Experiment 01 stands out, where the maximum force applied in the X-direction, at 15.24 N, was complemented by a spindle speed of 65,000 RPM, resulting in a remarkably fine surface roughness value of 2.981 µm. Conversely, Experiment 08 presented a unique scenario with a negative Y-direction force of -25.6 N and a positive X-direction force of 23.5 N. These force variations, when paired with a spindle speed of 42,000 RPM, yielded a roughness value of 3.672 µm. This intricate interplay between force directions and spindle speed showcases the nuanced impact of input parameters on surface roughness (as depicted in Figure-14).

Intriguingly, at 42,000 RPM and a feed rate of 50 mm/sec, the use of an Alt Diamond Cut tool geometry resulted in the minimal roughness value of 2.23 µm. This achievement coincided with the application of a maximum force of 23.6 N in the X-direction. Experiment 4 has the highest roughness Ra (3.768 µm) among all experiments and exhibits significantly higher force and torque values. This demonstrates that a rougher work-piece surface requires more force and torque to achieve the desired finish.

ISSN (Online) 2456-1290

International Journal of Engineering Research in Mechanical and Civil Engineering (IJERMCE)

Vol 10, Issue 10, October 2023

IV. FACTORS AFFECTING ROUGHNESS:

These findings emphasize the intricate relationship between spindle speeds, feed rate, tool geometry, and force application in shaping the surface roughness profile. The average roughness values, spanning from 2.2 µm to 3.7 µm, highlight the versatility of this robotic deburring setup in achieving a range of surface finishes (Figure 14).

Table 3: Variation in Average Roughness, force and torque with change of Input parameters.

Exp. No.	Input			Output						
				Roughness R_a (µm)	Force (N)			Torque (Nm)		
	Spindle Speed (RPM)	Feed Rate (mm/ sec)	Tool Geometry		F_x	F_y	F_z	T_x	T_y	T_z
1	65000	50	Double Cut	2.981	15.24	2.9	4.7	0.7	3.2	0.15
2	65000	38.8	Double Cut	2.386	13.5	2.7	3.2	0.55	3.2	0.17
3	65000	38.8	Alt Diamond Cut	2.615	25.7	-28.5	3.2	6.8	6.2	-0.06
4	65000	50	Alt Diamond Cut	3.768	24.5	-56.7	16.6	2.2	5.2	-1.65
5	42000	50	Alt Diamond Cut	2.232	23.6	-5.2	0.7	3.5	5.2	0.4
6	42000	38.8	Alt Diamond Cut	2.479	30.6	-18.5	0.711	5.2	6.2	0.05
7	42000	50	Double Cut	2.592	130.7	-91.2	197.6	8.1	8.2	0.02
8	42000	38.8	Double Cut	3.672	23.5	-25.6	6.5	4.7	4.6	-1.2

Furthermore, the variation in force values, ranging from 13.5 N to 130.7 N in the X-direction, underscores the dynamic nature of force application influenced by input parameters. These variations in force, as show in Figure 13, manifest as distinct and finely detailed average roughness profiles. The interplay between RPM, feed rate, and tool geometry demonstrates the complex and multifaceted nature of achieving specific surface finishes in robotic deburring processes, offering valuable insights for precision manufacturing and quality control.

Taguchi Analysis, a powerful statistical technique, is employed here to systematically study the relationship between torque (measured in Newton-meters) and several crucial machining parameters: spindle speed (in revolutions per minute, rpm), feed rate (measured in millimeters per second, mm/sec), and tool geometry. This analysis allows for a comprehensive understanding of how variations in these key factors impact torque during machining processes. By optimizing these parameters using Taguchi's robust experimental design principles, manufacturers can enhance their machining operations, improve product quality, and minimize energy consumption, ultimately leading to more efficient and cost-effective production processes.

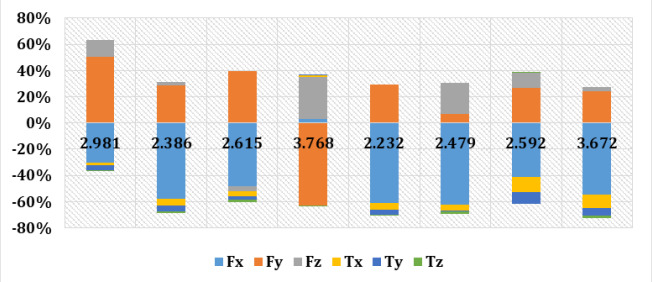

Figure 14: Force & Torque Calculation

The meticulous calculation of force and torque dynamics throughout the deburring process yields a wealth of data that encapsulates the nuanced interactions between the deburring tool and the workpiece. This dataset is marked by a spectrum of values, encompassing both positive and negative magnitudes, all meticulously referenced against the input parameters that govern the operation. These force and torque values serve as a window into the intricate mechanics at play during deburring. Conversely, the presence of negative values suggests forces or torques acting in the opposite direction, potentially indicating instances of resistance or counteractive forces within the system. These negative values often merit a closer examination, as they can provide crucial insights into areas where the deburring process may encounter challenges or inefficiencies.

By conducting a thorough analysis of these positive and negative values within the context of the input parameters, engineers and operators can gain invaluable insights into the efficiency, precision, and overall quality of the deburring operation. This analytical approach allows for the fine-tuning of the process, ensuring that forces and torques are optimally directed to achieve the desired results while minimizing any detrimental effects. The graphical representation of these dynamics, as illustrated in Figure-14, provides a visual aid in comprehending the intricate interplay between force, torque, and input parameters, enhancing the overall understanding of the deburring process's mechanics and performance.

Figure-15, which presumably contains additional graphical representations or data, likely serves as a complementary resource, further elucidating the complex dynamics at play during the deburring operation. This holistic approach to data analysis and visualization is invaluable for precision manufacturing, quality control, and process optimization, ultimately contributing to the consistent and high-quality execution of deburring tasks.

In summary, the data suggests complex interactions

between the input parameters (spindle speed, feed rate and tool geometry) and the output parameters (surface roughness, force and torque). The relationships between these variables are not linear, and multiple factors contribute to variations in the force and torque values observed in the experiments. Further analysis and experimentation may be needed to precisely characterize these relationships and optimize the deburring process for specific applications.

V. CONCLUSION

With the study of all 8 experiments the main conclusion are derived from study is:

i. Robotic deburring operation was successfully performed with L8 orthogonal array.
ii. After the deburring operation, the average roughness values noted in the range of 2.2 µm to 3.7 µm.
iii. Experiment 1 (higher feed rate) exhibits higher force values (Fx, Fy, Fz) compared to Experiment 2 (lower feed rate), indicating that an increase in feed rate generally leads to higher cutting forces.
iv. Experiments 3, 4, 5, 6, 7, and 8 all use "Alt Diamond Cut" tool geometry, but their input and output values vary significantly. This indicates that tool geometry alone is not the sole determinant of force and torque; other factors such as roughness Ra and feed rate play critical roles.
v. The applied force by the manipulator (~130N) is not mandatory for the deburring that increases the torque value respectively but gave a medium roughness profile of 2.52µm.

REFERENCES

[1] A. Verl, A. Valente, S. Melkote, C. Brecher, E. Ozturk, and L. T. Tunc, "Robots in machining," *CIRP Ann.*, 2019, doi: 10.1016/j.cirp.2019.05.009.
[2] J. M. Schimmels, "Multidirectional compliance and constraint for improved robotic deburring. Part 2: Improved bracing," *Robot. Comput. Integr. Manuf.*, 2001, doi: 10.1016/S0736-5845(00)00060-0.
[3] X. Ke *et al.*, "Review on robot-assisted polishing: Status and future trends," *Robotics and Computer-Integrated Manufacturing*. 2023. doi: 10.1016/j.rcim.2022.102482.
[4] A. Kuss, M. Drust, and A. Verl, "Detection of Workpiece Shape Deviations for Tool Path Adaptation in Robotic Deburring Systems," in *Procedia CIRP*, 2016. doi: 10.1016/j.procir.2016.11.094.
[5] J. Schmidt, F. Grandi, M. Peruzzini, R. Raffaeli, and M. Pellicciari, "Novel robotic cell architecture for zero defect intelligent deburring," in *Procedia Manufacturing*, 2020. doi: 10.1016/j.promfg.2020.10.021.
[6] J. N. Pires, "Force control experiments for industrial applications: A test case using an industrial deburring example," *Assem. Autom.*, 2007, doi: 10.1108/01445150710733414.
[7] F. Leo Princely and T. Selvaraj, "Vision assisted robotic deburring of edge burrs in cast parts," in *Procedia Engineering*, 2014. doi: 10.1016/j.proeng.2014.12.344.
[8] V. Shukla, V. Kumar, and A. Dixit, "Microstructural characteristics and tensile properties of ER70S-6 manufactured by Robotic CMT wire-and-arc additive manufacturing," *Mater. Today Proc.*, 2023, doi: 10.1016/j.matpr.2023.02.011.
[9] Z. Wang, Z. Li, J. He, J. Yao, and Y. Zhao, "Optimal design and experiment research of a fully pre-stressed six-axis force/torque sensor," *Meas. J. Int. Meas. Confed.*, 2013, doi: 10.1016/j.measurement.2013.03.003.
[10] W. Caesarendra, T. Wijaya, T. Tjahjowidodo, B. K. Pappachan, A. Wee, and M. I. Roslan, "Adaptive neuro-fuzzy inference system for deburring stage classification and prediction for indirect quality monitoring," *Appl. Soft Comput. J.*, 2018, doi: 10.1016/j.asoc.2018.01.008.
[11] A. Winkler and J. Suchý, "Robot force/torque control in assembly tasks," in *IFAC Proceedings Volumes (IFAC-PapersOnline)*, 2013. doi: 10.3182/20130619-3-RU-3018.00161.
[12] W. R. MacMillan, R. A. Irani, and M. Ahmadi, "Planar image-space trajectory planning algorithm for contour following in robotic machining," *CIRP J. Manuf. Sci. Technol.*, vol. 42, pp. 1–11, 2023, doi: 10.1016/j.cirpj.2023.01.005.
[13] S. Lloyd, R. Irani, and M. Ahmadi, "Application of Pseudo-Symbolic Dynamic Modeling (PSDM) in the Modeling & Calibration of a 6-DOF Articulated Robot," in *IFAC-PapersOnLine*, 2022. doi: 10.1016/j.ifacol.2022.11.164.
[14] J. E. Solanes, L. Gracia, P. Muñoz-Benavent, J. Valls Miro, V. Girbés, and J. Tornero, "Human-robot cooperation for robust surface treatment using non-conventional sliding mode control," *ISA Trans.*, 2018, doi: 10.1016/j.isatra.2018.05.013.
[15] A. García, L. Gracia, J. E. Solanes, V. Girbés-Juan, C. Perez-Vidal, and J. Tornero, "Robotic assistance for industrial sanding with a smooth approach to the surface and boundary constraints," *Comput. Ind. Eng.*, 2021, doi: 10.1016/j.cie.2021.107366.
[16] M. Guillo and L. Dubourg, "Impact & improvement of tool deviation in friction stir welding: Weld quality & real-time compensation on an industrial robot," *Robot. Comput. Integr. Manuf.*, 2016, doi: 10.1016/j.rcim.2015.11.001.
[17] J. Hu and P. R. Pagilla, "Dual-edge robotic gear chamfering with registration error compensation," *Robot. Comput. Integr. Manuf.*, 2021, doi: 10.1016/j.rcim.2020.102082.
[18] S. Hjorth and D. Chrysostomou, "Human–robot collaboration in industrial environments: A literature review on non-destructive disassembly," *Robotics and Computer-Integrated Manufacturing*. 2022. doi: 10.1016/j.rcim.2021.102208.
[19] D. Mukherjee, K. Gupta, L. H. Chang, and H. Najjaran, "A Survey of Robot Learning Strategies for Human-Robot Collaboration in Industrial Settings," *Robotics and Computer-Integrated Manufacturing*. 2022. doi: 10.1016/j.rcim.2021.102231.
[20] J. Gotlih, M. Brezocnik, and T. Karner, "Stiffness-based cell setup optimization for robotic deburring with a rotary table," *Appl. Sci.*, 2021, doi: 10.3390/app11178213.
[21] H. Jia, X. Lu, D. Cai, Y. Xiang, J. Chen, and C. Bao, "Predictive Modeling and Analysis of Material Removal Characteristics for Robotic Belt Grinding of Complex Blade," *Appl. Sci.*, 2023, doi: 10.3390/app13074248.
[22] W. Guo, R. Li, Y. Zhu, T. Yang, R. Qin, and Z. Hu, "A robotic deburring methodology for tool path planning and process parameter control of a five-degree-of-freedom robot manipulator," *Appl. Sci.*, 2019, doi: 10.3390/app9102033.